J. Fluid Mech. (2008), *vol.* 596, *pp.* 143–167. © 2008 Cambridge University Press
doi:10.1017/S0022112007009366 Printed in the United Kingdom

On weakly nonlinear convection in mushy layers during solidification of alloys

B. S. OKHUYSEN[1] AND D. N. RIAHI[2]

[1]Los Alamos National Laboratory, Los Alamos, NM87545, USA

[2]Department of Mathematics, 1201 West University Drive, University of Texas-Pan American, Edinburg, TX 78541-2999, USA

(Received 14 January 2007 and in revised form 1 September 2007)

We consider the problem of weakly nonlinear buoyant convection in horizontal mushy layers with permeable mush–liquid interface during the solidification of binary alloys. We analyse the effects of several parameters of the problem on the stationary modes of convection in the form of either a hexagonal pattern or a non-hexagonal pattern such as rolls, rectangles and squares. No assumption is made on the thickness of the mushy layer, and a number of simplifying assumptions made in previous theoretical investigations of the problem are relaxed here in order to study the problem based on a more realistic model. Using both analytical and numerical methods, we determine the steady solutions for the nonlinear problem in a range of the Rayleigh number R near its critical value. Both the nonlinear basic state and variable permeability of the present problem favour hexagon-pattern convection. The results of the analyses and computations indicate that depending on the range of values of the parameters, bifurcation to hexagonal or non-hexagonal convection can be either supercritical or subcritical. However, among all the computed solutions in the particular range of values of the parameters that are most relevant to those of the experiments, only convection in the form of down-hexagons with downflow at the cell centres and upflow at the cell boundaries, was found to be realizable, in the sense that its amplitude increases with R.

1. Introduction

The present study considers the problem of finite-amplitude steady convection in horizontal mushy layers during the directional solidification of binary alloys. The investigation is based on combined analytical and numerical methods for solving the governing equations, which were first derived by Hills, Loper & Roberts (1983) and later by Worster (1992) in the context of a two-layer system, in order to determine qualitative results about buoyant convection in mushy layers. The novel aspects of the present study are that a number of simplifying assumptions, which were made in previous linear and weakly nonlinear analyses of the problem (Fowler 1985; Amberg & Homsy 1993; Emms & Fowler 1994; Anderson & Worster 1995; Chung & Chen 2000), are no longer needed and, the present results are expected to be more realistic.

Hills *et al.* (1983) developed a set of thermodynamic equations for a mushy layer and then solved a simplified set of those equations approximately for the constrained growth of a binary alloy. Fowler (1985) developed a mathematical model for a mushy layer and analysed a simple mushy layer with constant permeability and with no coupling between the convective flow and the solidification. Worster (1992) solved the linear instability problem for a binary-alloy solidification system consisting of

a horizontal mushy layer and an overlying liquid layer. He detected two distinct modes of instability, one of which has been referred to as the mushy-layer mode. This mode drives the convective flow from the interior of the mushy layer and is the one responsible for the development of the chimneys within the mushy layer. This result is in agreement with the experimental result (Tait & Jaupart 1992) and is the main basis for the development of the present model as well as for the earlier analytical one (Amberg & Homsy 1993).

The simplified mushy-layer model for a weakly nonlinear study was introduced first by Amberg & Homsy (1993). The model was based on a near eutectic approximation and in the limit of large far-field temperature. It was used to examine the dynamics of the mushy layer in the regime of small deviation from the classical system of convection in a horizontal porous layer of constant permeability. To construct such a single-layer model for the mushy zone, Amberg & Homsy (1993) made a number of simplifying assumptions including those stated above and that the thickness δ of the mushy layer is sufficiently small and the layer is totally isolated from the overlying liquid layer. In addition, they assumed that the amplitude ε of convection is of the same order as δ. The finite-amplitude steady convection studied by Amberg & Homsy (1993) was limited to two-dimensional rolls and hexagons only. The authors found that two-dimensional rolls were supercritical for sufficiently small values of the deviation of the permeability from a constant value and subcritical if such deviation was not too small, and steady hexagons were found to be transcritical.

Anderson & Worster (1995) used the basic model due to Amberg & Homsy (1993), but extended the analytical studies to the limit of large Stefan number S, which represents the latent heat release due to solidification, and the case $\varepsilon \ll \delta \ll 1$. They applied a double-series expansion in powers of ε and δ for the rescaled variables and the Rayleigh number R. They focused on the steady modes of convection and calculated, in particular, the finite-amplitude steady solutions in the form of two-dimensional rolls and hexagons.

Chung & Chen (2000) modified the boundary conditions of the Amberg & Homsy (1993) model, replacing the condition of no vertical volume flux at the top boundary by a condition of constant pressure. This alteration results in a mushy layer that is more coupled to the upper melt layer. They found better agreement with the results of the linear study for the two-layer system (Worster 1992).

Tait, Jahrling & Jaupart (1992) carried out carefully controlled laboratory experiments on a water–ammonium chloride solution in a square tank. In the early stages of their experiments, they observed hexagonal planform of convection in the mushy layer near the onset of motion. The flow structure was observed to be in the form of down-hexagonal cells in the sense that upflow occurred mainly at the cell boundaries and downflow at the cell centres.

The weakly nonlinear analyses carried out in the past, which were described briefly earlier in this section, were based on a number of unrealistic assumptions such as that of a thin mushy layer, and the results for the planform of convection were not generally consistent with the corresponding experimental observations.

Here, a weakly nonlinear analysis of buoyant convection in a more realistic mushy-layer model is undertaken by removing a number of simplifying and unrealistic assumptions that were made in previous nonlinear analyses of the problem in order to establish a better model in predicting results that validate the main experimental results and can be used in applications such as that of controlling chimney convection within a mushy layer, which is known to lead to a class of defects called freckles in the solidified alloy (Copley *et al.* 1970).

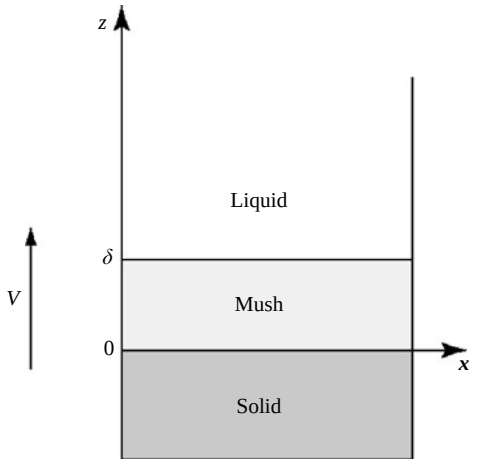

FIGURE 1. This is a schematic diagram for the physical system.

Sections 2 and 3 deal with the mathematical formulation of the problem and the analyses. The results are presented and discussed in § 4, which is followed by the conclusion and some remarks in § 5.

2. Mathematical formulation

2.1. *The model*

We consider a binary alloy melt that is cooled from below and the denser alloy is solidified at a constant speed V. Owing to the solidification process, a distinct mushy layer which is composed of a mixture of melt and solid dendrites forms between a lower solidified material and an upper liquid melt (figure 1). The overlying liquid melt is assumed to have a composition $C_0 > C_E$ and temperature $T_\infty > T_L(C_0)$ far above the mushy layer, where C_E is the eutectic composition and T_L is the local liquidus temperature (Worster 1991).

Following Worster (1991), the mushy layer is assumed to be in a state of thermodynamic equilibrium so that

$$\tilde{T} = T_L(C_0) + \Gamma(\tilde{C} - C_0), \tag{1}$$

Where $\tilde{T}$ is the temperature, $\tilde{C}$ is the composition and Γ is the constant slope of the liquidus. We consider the solidifying system in a moving frame of reference ox' y' z', whose origin lies on the solidification front and translating at speed V with the solidification front in the positive z'-direction (figure 1), which is anti-parallel to the gravity vector.

We model the mushy layer as a porous medium where Darcy's law holds, and, when the Oberbeck–Boussinesq approximation is applied, conservation of mass, momentum, heat and composition can be written as the corresponding dimensional equations (Worster 1991). Conditions for a mushy layer to exist, its thickness d to be dictated and the conditions at the mush–liquid interface are all given in Worster (1991) and will not be repeated here. Here, the mush–liquid interface is assumed to be permeable and with the temperature maintained at the liquidus temperature.

A hybrid of the single- and double-layer approaches is developed into the model presented here. We retain the decoupling of the liquid and mushy regions, so that only the mushy region is considered. However, we presuppose the existence of the

upper liquid region and apply an integration procedure, which was described and used in Worster (1991) in the limit of sufficiently small solute diffusion, to obtain the mushy-layer thickness in terms of the characteristic length due to the thermal diffusion. This approach has also been taken for studying linear stability in the two-layer model (Worster 1992; Chen, Lu & Yang 1994). Our weakly nonlinear approach is then a standard one, which is based on a combination of a perturbation technique for small-amplitude parameter ε and some numerical integration.

2.2. *Non-dimensional system*

The governing equations are non-dimensionalized by using V, κ/V, κ/V^2, $\beta\Delta C\rho_0 g\kappa/V$, ΔC and ΔT as scales for velocity, length, time, pressure, solute and temperature, respectively. Here κ is the thermal diffusivity, g is acceleration due to gravity, ρ_0 is a reference density, $\beta = \beta^* - \Gamma\alpha^*$, where α^* and β^* are the expansion coefficients for the heat and solute, respectively, $\Delta C = C_0 - C_E$, $\Delta T = T_L(C_0) - T_E$ and T_E is the eutectic temperature. The non-dimensional form of the equations for momentum, continuity, temperature and solute concentration are then

$$\tilde{K}(\tilde{\chi})\tilde{\boldsymbol{u}} = -\nabla\tilde{p} - R\tilde{\theta}\boldsymbol{e}_z, \tag{2a}$$

$$\nabla\cdot\tilde{\boldsymbol{u}} = 0, \tag{2b}$$

$$(\partial/\partial t - \partial/\partial z)[\tilde{\theta} - S(1-\tilde{\chi})] + \tilde{\boldsymbol{u}}\cdot\nabla\tilde{\theta} = \nabla^2\tilde{\theta}, \tag{2c}$$

$$(\partial/\partial t - \partial/\partial z)[\tilde{\chi}\tilde{\theta} + C(1-\tilde{\chi})] + \tilde{\boldsymbol{u}}\cdot\nabla\tilde{\theta} = \varepsilon_{\mathrm{m}}\nabla^2\tilde{\theta}, \tag{2d}$$

where $\tilde{\boldsymbol{u}} = \tilde{u}\boldsymbol{e}_x + \tilde{v}\boldsymbol{e}_y + \tilde{w}\boldsymbol{e}_z$ is the volume flux vector per unit area, which is also known as the Darcy velocity vector (Joseph 1976), $\tilde{\boldsymbol{u}}$ and $\tilde{v}$ are the horizontal components of $\tilde{\boldsymbol{u}}$ along the horizontal x- and y-directions, respectively, $\boldsymbol{e}_x$ and $\boldsymbol{e}_y$ are unit vectors along the positive x- and y-directions, $\tilde{w}$ is the vertical component of $\tilde{\boldsymbol{u}}$ along the z-direction, $\boldsymbol{e}_z$ is a unit vector along the positive z-direction, $\tilde{p}$ is the modified pressure, $\tilde{\theta}$ is the non-dimensional composition, or equivalently temperature (Worster 1992), $\tilde{\theta} = [\tilde{T} - T_L(C_0)]/\Delta T = (\tilde{C} - C_0)/\Delta C$, t is the time variable, $\tilde{\chi}$ is the local liquid fraction or porosity, $R = \beta\Delta C g\Pi(1)/(V_0\nu)$ is the Rayleigh number, $\Pi(1)$ is a reference value at $\tilde{\chi} = 1$ of the permeability $\Pi(\tilde{\chi})$ of the porous medium, which is assumed to be finite (Worster 1992), ν is the kinematic viscosity, $\tilde{K}(\tilde{\chi}) \equiv \Pi(1)/\Pi(\tilde{\chi})$, $\varepsilon_m = D_m/\kappa$ is the inverse of the Lewis number, $S = L/(C_m\Delta T)$ is the Stefan number, C_m is the specific heat per unit volume, L is the latent heat of solidification per unit volume, $C = (C_s - C_0)/\Delta C$ is a concentration ratio and C_s is the composition of the solid phase forming the dendrites. Following Worster (1991), we assume that temperature equilibrates much faster than mass, so that $\varepsilon_m = 0$ is considered for all the analyses and the results herein.

The governing equations (2*a*)–(2*d*) are subject to the following boundary conditions:

$$\tilde{\theta} + 1 = \tilde{w} = 0 \quad \text{at } z = 0, \tag{3a}$$

$$\tilde{\theta} = 1 - \tilde{\chi} = \partial\tilde{w}/\partial z = 0 \quad \text{at } z = \delta, \tag{3b}$$

where $\delta = dV/\kappa$ is a growth Péclet number representing the dimensionless depth of the layer. The boundary conditions (3*a*) as well as those given in (3*b*) for the temperature and liquid fraction at $z = \delta$ are the same as the corresponding ones for a two-layer system (Worster 1992). The condition $\partial\tilde{w}/\partial z = 0$ in (3*b*) is the one used by Chung & Chen (2000) on the permeable upper boundary. This condition can be derived easily from (2*a*)–(2*b*) by assuming the constant pressure condition that was assumed by Chung & Chen (2000) on the upper boundary. For the constant

pressure condition, (2*a*) yields $\partial\tilde{\boldsymbol{u}}/\partial x = \partial\tilde{v}/\partial y = 0$, and (2*b*) then implies $\partial\tilde{w}/\partial z = 0$. A physical justification for using such a permeable boundary condition is briefly given as follows. For a two-layer system (Worster 1992), the condition of the continuity of pressure, which holds across the mush–liquid interface, leads to a boundary condition on this interface that was derived and given in Worster (1992), and such a boundary condition is reduced to $\partial\tilde{w}/\partial z = 0$ in the limit of sufficiently small Darcy number $D_a = \Pi(1)/d^2$. As Worster (1992) noted, D_a can represent the square of the ratio of the average spacing between dendrites to the thermal length scale, and such a ratio is typically very small.

The permeability relation is $\tilde{K}(x, y, z, t) = \Pi(1)/\Pi(\tilde{\chi})$ and the permeability $\Pi(\tilde{\chi})$ is derived from $\Pi(\tilde{\chi}) = \tilde{\chi}^3$ (x, y, z, t) to obtain

$$\tilde{K} = \tilde{\chi}^{-3}, \tag{4}$$

where $\tilde{K}$ decreases with increasing $\tilde{\chi}$, which is physically realistic. Equation (4) resembles a Kozeny-type equation for the variable permeability in which the specific volumetric surface area of the phase boundaries is considered to be constant (Lage 1998). This variable permeability model, which has been used before in related studies (Worster 1992; Emms & Fowler 1994), is related to the experimentally observed variable permeability cases in porous media and is the modelling assumption for the permeability in the present study.

3. Analyses

3.1. *Steady basic-state and perturbation systems*

The basic-state system is considered to be motionless, and the corresponding quantities are designated by subscript '*b*' and are assumed to be at most a function of z.

$$\tilde{\theta} = \theta_b(z) + \varepsilon\theta(x, y, z, t), \tag{5a}$$

$$\tilde{\chi} = \chi_b(z) + \varepsilon\chi(x, y, z, t), \tag{5b}$$

$$\tilde{\boldsymbol{u}} = \boldsymbol{u}_b + \varepsilon\boldsymbol{u}(x, y, z, t), \quad \boldsymbol{u}_b \equiv 0, \tag{5c}$$

$$\tilde{p} = p_b(z) + \varepsilon p(x, y, z, t), \tag{5d}$$

$$\tilde{K} = K_b(\chi_b) + \varepsilon K(\chi), \tag{5e}$$

where the small deviation of each dependent variable from its basic-state quantity, which is the perturbation quantity whose magnitude is measured by the perturbation amplitude ε, can vary with respect to spatial and time variables, as is evident from (5*a*)–(5*e*).

Using (5*a*)–(5*e*) in (2*a*)–(2*d*) and (3*a*)–(3*b*) and setting all the perturbation quantities to be zero, we find the following system of equations and boundary conditions for the basic state:

$$\mathrm{d}^2\theta_b/\mathrm{d}z^2 + \mathrm{d}\theta_b/\mathrm{d}z + S\,\mathrm{d}\chi_b/\mathrm{d}z = 0, \quad \chi_b\mathrm{d}\theta_b/\mathrm{d}z + (\theta_b - C)\,\mathrm{d}\chi_b/\mathrm{d}z = 0, \quad \mathrm{d}p_b/\mathrm{d}z = -R\theta_b, \tag{6a–c}$$

$$\theta_b = -1 \text{ at } z = 0, \quad \theta_b = \chi_b - 1 = 0 \text{ at } z = \delta. \tag{6d–e}$$

Using (6), we integrate the heat and solute equations once, apply the boundary conditions and then substitute the expression for χ_b into the integrated form of the heat equation, integrate and apply the boundary conditions again to determine the basic-state solutions. However, these solutions would then depend on the mushy-layer thickness δ, which appears so far as an arbitrary parameter. To concentrate on the

most realistic possible solutions, we made use of the results of Worster (1991, 1992) for the basic-state solutions in the upper liquid region in the limit of $\varepsilon_m = 0$ and found the condition $\mathrm{d}\theta_b/\mathrm{d}z = \theta_\infty$ at the mush–liquid interface. Here, $\theta_\infty = [T_\infty - T_L(C_0)]/\Delta T$ is the non-dimensional far-field temperature. Using this condition, which represents the continuity of the heat flux across the mush–liquid interface, in place of zero basic-state temperature at $z = \delta$, we find the following results for the basic-state solutions:

$$z(\theta_b) = [(a_1 - C)/(a_1 - a_2)] \ln [(1 + a_1)/(a_1 - \theta_b)] + [(C - a_2)/(a_1 - a_2)] \times \ln[(1 + a_2)/(a_2 - \theta_b)], \tag{7a}$$

where

$$a_1 = (A_1 + \sqrt{A_2})/2, \quad a_2 = (A_1 - \sqrt{A_2})/2, \; A_1 = (S + C + \theta_\infty), \quad A_2 = \left(A_1^2 - 4C\theta_\infty\right), \tag{7b–e}$$

and

$$\chi_b = C/(C - \theta_b), \quad p_b = -R \int \theta_b \, \mathrm{d}z + p_0, \tag{8a,b}$$

where p_0 is a constant.

To determine the thickness of the mushy layer, δ, we use the remaining condition in (6*e*) for the basic-state temperature at the upper boundary by replacing θ_b and z in (7*a*) with 0 and δ, respectively. Thus, the following expression for δ is obtained as functions of the system parameters C, S and θ_∞:

$$\delta = [(a_1 - C)/(a_1 - a_2)] \ln [(1 + a_1)/a_1] + [(C - a_2)/(a_1 - a_2)] \ln [(1 + a_2)/a_2]. \tag{9}$$

Using (5*b*) and (5*e*) in (4), we find

$$K_b = \chi_b^{-3}, \tag{10}$$

$$K \sim -3\chi_b^{-4}\left[\chi - 2\varepsilon\chi_b^{-1}\chi^2\right]. \tag{11}$$

For the analysis of the perturbation system, it is convenient to use the general representation

$$\boldsymbol{u} = \Omega P + \boldsymbol{E}\psi, \tag{12a}$$

$$\Omega \equiv \nabla \times \nabla \times \boldsymbol{e}_z, \quad \boldsymbol{E} \equiv \nabla \times \boldsymbol{e}_z, \tag{12b–c}$$

for the divergent-free vector field $\boldsymbol{u}$ (Chandrasekhar 1961). Here, P and ψ are the poloidal and toroidal functions for $\boldsymbol{u}$, respectively. By taking the vertical component of the curl of (2*a*) it can be shown that the toroidal part $\boldsymbol{E}\psi$ of $\boldsymbol{u}$ must vanish. Taking the vertical components of the double curl of (2*a*) and using (2*b*) and (5)–(6) in (2)–(3), we find the following system for the perturbation quantities, which will be analysed in this section,

$$\varepsilon[\nabla^2(K\Delta_2 P) + (\partial/\partial z)(\Omega P \cdot \nabla K)] + [K_b\nabla^2 + (\mathrm{d}K_b/\mathrm{d}z)(\partial/\partial z)]\Delta_2 P - R\Delta_2\theta = 0, \tag{13a}$$

$$(\partial/\partial t - \partial/\partial z - \nabla^2)\theta + S(\partial/\partial t - \partial/\partial z)\chi - (\mathrm{d}\theta_b/\mathrm{d}z)\Delta_2 P = -\varepsilon(\Omega P)\cdot\nabla\theta, \tag{13b}$$

$$[\chi_b(\partial/\partial t - \partial/\partial z) - \mathrm{d}\chi_b/\mathrm{d}z]\theta + [(\theta_b - C)(\partial/\partial t - \partial/\partial z) - (\mathrm{d}\theta_b/\mathrm{d}z)]$$
$$\chi - (\mathrm{d}\theta_b/\mathrm{d}z)\Delta_2 P = -\varepsilon[(\Omega P)\cdot\nabla\theta + \chi(\partial/\partial t - \partial/\partial z)\theta + \theta(\partial/\partial t - \partial/\partial z)\chi], \tag{13c}$$

$$\theta = P = 0 \quad \text{at} \quad z = 0, \tag{14a}$$

$$\theta = \partial P/\partial z = \chi = 0 \quad \text{at} \quad z = \delta, \tag{14b}$$

where

$$\Delta_2 \equiv \partial^2/\partial x^2 + \partial^2/\partial y^2.$$

It will be useful to define the vectorial notation $\boldsymbol{q} = (\theta,\ \chi,\ P)^T$ and introduce the linear operators $\boldsymbol{L}$ and $\boldsymbol{L}'$ and the nonlinear operator $\boldsymbol{N}$, defined by (A 1)–(A 3) in the Appendix, to represent the perturbation equations (13) succinctly as

$$(\boldsymbol{L} - R\boldsymbol{L}')\boldsymbol{q} = \varepsilon \boldsymbol{N}(\boldsymbol{q}, \boldsymbol{q}). \tag{15}$$

The boundary conditions (14) can then be represented as

$$\boldsymbol{B}[\boldsymbol{q}(z=0),\quad \boldsymbol{q}(z=\delta)] = 0, \tag{16}$$

where $\boldsymbol{q}(z=0)$ and $\boldsymbol{q}(z=\delta)$ mean (14*a*) and (14*b*), respectively.

3.2. *Linear stability analysis*

Designating the linear solution by $\boldsymbol{q}_0$ and setting $\varepsilon = 0$ in (15)–(16), we find the linear system for the perturbations

$$(\boldsymbol{L} - R\boldsymbol{L}')\boldsymbol{q}_0 = 0, \quad \boldsymbol{B}_0[\boldsymbol{q}_0(z=0),\quad \boldsymbol{q}_0(z=\delta)] = 0. \tag{17a,b}$$

Since the coefficients in (17*a*) are functions of z only, the normal mode approach (Chandrasekhar 1961) is used to express $\boldsymbol{q}_0$ in the form

$$\boldsymbol{q}_0 = \tilde{\boldsymbol{q}}_0(z) H(x, y) \exp(\sigma t), \tag{18}$$

where σ is the growth rate of the perturbations and the function $H(x, y)$ satisfies

$$\Delta_2 H = -\tilde{\alpha}^2 H. \tag{19}$$

Here the planform function H is given by

$$H(x, y) = \sum_{n=-N}^{N} A_n H_n, \quad H_n \equiv \exp(\mathrm{i}\alpha_n \cdot \boldsymbol{r}), \tag{20a,b}$$

i is the pure imaginary number ($\mathrm{i} = \sqrt{-1}$), subscript n takes only non-zero integer values from $-N$ to N, N is a positive integer representing the number of distinct modes, $\boldsymbol{r}$ is the position vector, and the horizontal wavenumber vectors α_n satisfy the properties

$$\alpha_n \cdot \boldsymbol{e}_z = 0, \quad |\alpha_n| = \tilde{\alpha}, \quad \alpha_{-n} = -\alpha_n \tag{21}$$

(Busse 1967). The coefficients A_n are constants and satisfy the conditions

$$\sum_{n=-N}^{N} A_n A_n^* = 1, \quad A_{-n} = A_n^*, \tag{22a,b}$$

where the asterisk indicates the complex conjugate. The z-dependent coefficient $\tilde{\boldsymbol{q}}_0$ in (18) satisfies an equation of the form (17*a*), provided $\partial/\partial t$, $\partial/\partial z$, R, Δ_2 and ∇^2 in $\boldsymbol{L}$ and $\boldsymbol{L}'$ are replaced, respectively, by σ, $\mathrm{D} \equiv \mathrm{d}/\mathrm{d}z$, $\tilde{R}_0$, $-\tilde{\alpha}^2$ and $(\mathrm{D}^2 - \tilde{\alpha}^2)$, where $\tilde{R}_0$ is the Rayleigh number for the linear problem.

For each wavenumber $\tilde{\alpha}$, a marginal Rayleigh number $\tilde{R}_0$ is computed at which $\sigma = 0$. The result may be plotted to obtain a neutral stability curve. In this paper, we are interested only in the minimum value R_0 of the Rayleigh number $\tilde{R}_0$ on the neutral stability curve, which is achieved at a particular value α of the wavenumber $\tilde{\alpha}$.

3.3. *Nonlinear analysis*

3.3.1. *Adjoint system*

In order to compute the solvability conditions for the nonlinear systems, the solutions to the adjoint linear problem are required. Since solution to (17) has the

form given in (18) with the planform function H of the form (20a), the solution $\boldsymbol{q}_0^{(a)} \equiv (\theta_0^{(a)}, \chi_0^{(a)}, P_0^{(a)})$ to the corresponding adjoint problem has the form

$$\boldsymbol{q}_0^{(a)} = \sum_{n=-N}^{N} \boldsymbol{q}_{0n}^{(a)}, \quad \boldsymbol{q}_{0n}^{(a)} = \left(\theta_{0n}^{(a)}, \chi_{0n}^{(a)}, P_{0n}^{(a)}\right)^T = \tilde{\boldsymbol{q}}_0^{(a)}(z) A_n H_n(x, y), \tag{23a, b}$$

where the z-dependent coefficient function $\tilde{\boldsymbol{q}}_0^{(a)}(z) = [\tilde{\theta}_0^{(a)}(z),\ \tilde{\chi}_0^{(a)}(z),\ \tilde{P}_0^{(a)}(z)]^T$ is the solution of the adjoint linear system

$$\boldsymbol{L}^{(a)} \tilde{\boldsymbol{q}}_0^{(a)} = 0, \quad \boldsymbol{B}_0^{(a)} \left[\tilde{\boldsymbol{q}}_0^{(a)}(z=0), \quad \tilde{\boldsymbol{q}}_0^{(a)}(z=\delta)\right] = 0. \tag{24}$$

The linear operator $\boldsymbol{L}^{(a)}$ and the boundary condition $\boldsymbol{B}_0^{(a)}$ are defined by (A4) in the Appendix.

3.3.2. *Expansions*

The expansions for the perturbation quantities and R that are required up to the order ε^2 in the present analyses, are

$$(P, \theta, \chi, R) \sim \sum_{n=0}^{2} (P_n, \theta_n, \chi_n, R_n)\, \varepsilon^n. \tag{25a}$$

It should also be noted that in the present analyses, we must use the following expansion for K up to only order ε

$$K \sim K_0 + \varepsilon K_1, \tag{25b}$$

where it was found from (11) that

$$K_0 = -3\chi_b^{-4}\chi_0,\ K_1 = -3\chi_b^{-4}\left[\chi_1 - 2\chi_b^{-1}\chi_0^2\right]. \tag{25c, d}$$

3.3.3. *First-order problem*

At order ε, the perturbation system is derived from (15)–(16) and has the form

$$(\boldsymbol{L} - R_0\boldsymbol{L}')\boldsymbol{q}_1 = R_1\boldsymbol{L}'\boldsymbol{q}_0 + \boldsymbol{N}(\boldsymbol{q}_0, \boldsymbol{q}_0), \quad \boldsymbol{B}[\boldsymbol{q}_1(z=0) = 0, \boldsymbol{q}_1(z=\delta)] = 0. \tag{26a, b}$$

Consider the system (26). The solvability condition for this system is derived by multiplying (26a) by any particular solution $\boldsymbol{q}_{0n}^{(a)}$ of the adjoint linear system, using (26b) and averaging the resulting equation over the layer. It yields

$$R_1 = -\left\langle \boldsymbol{q}_{0n}^{(a)} \boldsymbol{N}(\boldsymbol{q}_0, \boldsymbol{q}_0) \right\rangle \Big/ \left\langle \boldsymbol{q}_{0n}^{(a)} \boldsymbol{L}' \boldsymbol{q}_0 \right\rangle, \tag{27}$$

where angle brackets indicates the average over the layer.

3.3.4. *Second-order problem*

We now consider the system (15)–(16) at order ε^2. It is

$$(\boldsymbol{L} - R_0\boldsymbol{L}')\boldsymbol{q}_2 = R_1\boldsymbol{L}'\boldsymbol{q}_1 + R_2\boldsymbol{L}'\boldsymbol{q}_0 + \boldsymbol{N}(\boldsymbol{q}_0, \boldsymbol{q}_1) + \boldsymbol{N}(\boldsymbol{q}_1, \boldsymbol{q}_0), \quad \boldsymbol{B}[\boldsymbol{q}_2(z=0), \boldsymbol{q}_2(z=\delta)] = 0. \tag{28a, b}$$

The solvability condition at this order yields

$$R_2 = \left\{-R_1\left\langle \boldsymbol{q}_{0n}^{(a)} \boldsymbol{L}' \boldsymbol{q}_1 \right\rangle - \left\langle \boldsymbol{q}_{0n}^{(a)} [\boldsymbol{N}(\boldsymbol{q}_0, \boldsymbol{q}_1) + \boldsymbol{N}(\boldsymbol{q}_1, \boldsymbol{q}_0)] \right\rangle\right\} \Big/ \left\langle \boldsymbol{q}_{0n}^{(a)} \boldsymbol{L}' \boldsymbol{q}_0 \right\rangle. \tag{29}$$

The system (22) together with (27) and (29), can be used to study the steady solutions in the form of two-dimensional rolls and three-dimensional cells. We shall restrict our attention to the simplest types of solution, which include those observed

in the applications. These solutions are called regular or semi-regular solutions (Busse 1967). In the case of a regular solution, all angles between two neighbouring α-vectors are equal to a value designated by γ in degrees, and (22) yields

$$|A_1|^2 = \cdots = |A_N|^2 = 1/(2N). \tag{30}$$

In the more general semi-regular solution, where (30) still holds, the scalar products between any of the α-vectors and its two neighbouring α-vectors assume the constant values α_1 and α_2. An example of a semi-regular solution is that due to rectangular cells ($N=2$), where $\alpha_1 = -\alpha_2$, and for each rectangular cell the angle between any two neighbouring wavenumber vectors, which both originate at the cell centre and each of which is directed toward a cell vertex, is either γ or $180^\circ - \gamma$. Regular solutions can follow from the semi-regular ones for the special case $\alpha_1 = \alpha_2$. Simple forms of regular solutions correspond to the cases of two-dimensional rolls ($N=1$), square cells ($N=2$) and hexagons ($N=3$).

The simplest types of solution, which turn out to be preferred under certain conditions in the present study, are described briefly as follows. For steady two-dimensional rolls, $N=1$, $A_n = 1/\sqrt{2}$ and the angle γ between the two wavenumber vector is 180°. For rectangular pattern convection, $N=2$, $A_n = 1/2$ and $\gamma \neq 90^\circ$. For square pattern convection, $N=2$, $A_n = 1/2$ and $\gamma = 90^\circ$. For hexagonal convection, $N=3$, $A_n = 1/\sqrt{6}$ and $\gamma = 60^\circ$ (Busse 1967, 1978). Since the right-hand side in the expression for R_1 given by (27) is found to be the sum of terms over subscripts k and p each of which is proportional to the integral expression of the form $\langle H_n H_k H_p \rangle$ that differ from zero only if

$$\alpha_n + \alpha_k + \alpha_p = 0 \tag{31}$$

for at least some k and p, then it can be seen that (31) cannot be satisfied for the already described non-hexagonal solutions and, thus, $R_1 = 0$ for such solutions, while generally $R_1 \neq 0$ for the hexagonal solutions since (31) can be satisfied in this case.

As will be referred to in § 4, the sign of the vertical motion at the cell centres for hexagons, which is determined by the sign of ε, is inferred from the condition

$$\varepsilon R_1 < 0 \tag{32a}$$

for the subcritical hexagons at order ε and from

$$\varepsilon R_1 > 0 \tag{32b}$$

for the supercritical hexagons at order ε. If the sign of the vertical motion at the cell centres for the hexagons is negative, such hexagons are referred to as down-hexagons, while up-hexagons refer to the case where the sign of the vertical motion is positive at the cell centres.

3.4. *Computation*

3.4.1. *Marginal stability problem*

In contrast to the previous analytical studies of the nonlinear convection in mushy layers that were referred to in § 1, here the equations for determining linear stability must be solved numerically. To solve the marginal stability problem, we used a multiple shooting technique (Keller 1976). First, we followed Worster (1992) by using the basic-state temperature as the independent variable instead of z in the linear system in order to avoid having to invert the transcendental equations for the basic state. The variable

$$\tau = -\theta_b \tag{33}$$

maps the computational domain of the mushy zone into the closed interval [0, 1]. In this mapping, $\tau = 0$ corresponds to the mush–liquid interface and the solid–mush interface is located at $\tau = 1$. We used such a change of variable to convert the ordinary differential system for $\tilde{\boldsymbol{q}}_0$ with independent variable z into a corresponding one with the independent variable τ. For a given set of parameters, the linear equation for the τ-dependent coefficient $\tilde{\boldsymbol{q}}_0$, subjected to given boundary conditions at $\tau = 0$ was integrated across the domain of the mushy layer, and the Rayleigh number was varied and the equation for $\tilde{\boldsymbol{q}}_0$ reintegrated until the boundary condition at $\tau = 1$ was satisfied. This led to an equation of the form $F(\tilde{R}_0, \tilde{\alpha}; \theta_\infty, C, S) = 0$ for the marginally stable states. From the latter equation and for given values of the parameters, the neighbourhood of the minimum value of the Rayleigh number was located and the marginal stability computations were further refined in this neighbourhood until the minimum value of $\tilde{R}_0$ with respect to $\tilde{\alpha}$ was found. Then the eigenfunctions $\tilde{\boldsymbol{q}}_0$ of the linear system at the critical Rayleigh number R_0 and wavenumber α were determined.

3.4.2. *Nonlinear problem*

After the minimum Rayleigh number and the corresponding wavenumber were found from the marginal stability problem, we solved the adjoint problem in τ using the same method of approach as in the case of the original linear problem. We checked the numerical integrity of the adjoint solutions by generating a neutral curve from the adjoint system. The validity was ensured when a neutral curve generated by the technique already described was computed based on the adjoint system and was found to be equal to the neutral stability curve based on the original linear system. After the adjoint solutions were found, we applied the solvability condition (27) to the order ε of the perturbation system to obtain the first-order correction R_1 to the Rayleigh number using Simpson integration. Next, we applied separation of variables and followed standard weakly nonlinear theory (Busse 1967) for the order ε of the perturbation system to determine the ordinary differential equations for the z-dependent parts of the dependent variables for each mode of the selected flow pattern. These equations are linear in the z-dependent parts of the dependent variables in the order ε and contain non-homogeneous terms due to z-dependent parts of the linear solution (18). Then, we used (33) to convert the resulting non-homogeneous system in the order ε into a system with the independent variable τ and solved for each mode of the selected flow pattern, the solutions of such a system in the τ-coordinate using the multiple shooting for the linear two-point boundary-value problems (Ascher, Mattheij & Russell 1995). The solution $\boldsymbol{q}_1$ was then determined for each mode of selected types of flow pattern. We then applied the solvability condition (29) to the order ε^2 of the perturbation system to obtain the second-order correction R_2 to the Rayleigh number by Simpson integration. It should be noted that to determine the results in the present qualitative study, accuracy to three decimal places was found to be sufficient for each numerical value computed, including the first- and higher-order corrections to the dependent variables and the Rayleigh number.

4. Results and discussion

4.1. *Effect of the far-field temperature on the linear system*

Here, the variation of the linear problem with respect to the far-field temperature θ_∞ is discussed. The parameters C and S are kept constant equal to one. The mushy-layer depth δ is plotted as a function of θ_∞ in figure 2. It can be seen that the mushy-layer

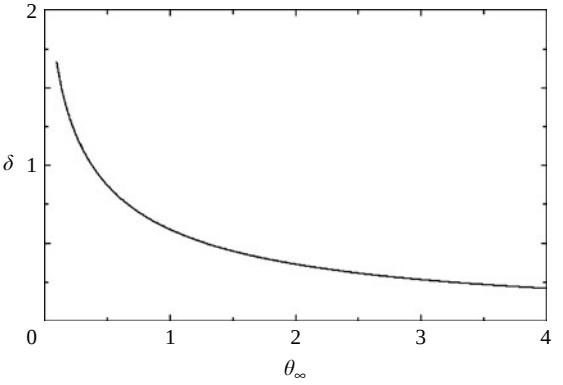

FIGURE 2. Variation of δ versus θ_∞ for $C = 1$ and $S = 1$.

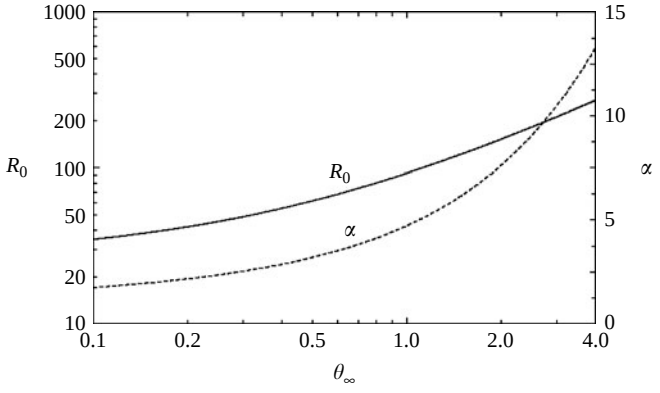

FIGURE 3. Variations of R_0 and α versus θ_∞ for $C = 1$ and $S = 1$.

thickness is reduced as the far-field temperature is increased, a result which was also noted by Worster (1992) for the two-layer system. The variations of the critical Rayleigh number and wavenumber versus θ_∞ are shown in figure 3. It is seen that R_0 and α increase with the far-field temperature. This result indicates that the flow is more stable and the flow structure can have a shorter horizontal length scale as θ_∞ increases.

4.2. *Nonlinear properties*

Owing to the degeneracy of the linear system, these linear results are applicable to both two- and three-dimensional convection cases whose nonlinear properties and results are now presented and discussed.

Important quantities due to the nonlinear effects are the coefficients R_1 and R_2, which are calculated in the present study. These coefficients represent leading contributions to the change in R required to obtain finite amplitude ε for a nonlinear solution. In terms of these coefficients, the amplitude of convection is of order

$$|\varepsilon| = \left\{\pm |R_1| \pm \left[R_1^2 + 4R_2(R - R_0)\right]^{0.5}\right\}/(2R_2). \tag{34}$$

As can be seen from (34), there are four expressions for $|\varepsilon|$ corresponding to plus and minus signs in front of the square-root term and plus and minus signs in front of the $|R_1|$ term in (34). For the case $\varepsilon R_1 < 0$, the two roots with plus sign in front of

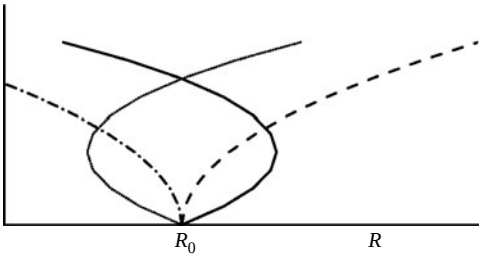

FIGURE 4. Bifurcation diagram (showing $|\varepsilon|$ versus R) for four cases (i) $\varepsilon R_1 > 0$, $R_2 > 0$ (dashed line), (ii) $\varepsilon R_1 > 0$, $R_2 < 0$ (solid line), (iii) $\varepsilon R_1 < 0$, $R_2 > 0$ (dotted line), (iv) $\varepsilon R_1 < 0$, $R_2 < 0$ (dash-dot line).

$|R_1|$ provide the expressions for $|\varepsilon|$, while the two roots with negative sign in front of $|R_1|$ provide the expressions for $|\varepsilon|$ if $\varepsilon R_1 > 0$. For either case $\varepsilon R_1 < 0$ or case $\varepsilon R_1 > 0$, the expression with the plus sign in front of the square-root term corresponds to the case where R_2 is positive, while the expression with negative sign in front of the square-root term corresponds to the case where R_2 is negative.

For sufficiently small $|\varepsilon|$, we may neglect the term $R_2\varepsilon^2$ in comparison to the term $R_1\varepsilon$ in the expression for R, which leads to the following expression for $|\varepsilon|$:

$$|\varepsilon| = \pm(R - R_0)/|R_1|, \tag{35}$$

where the plus sign corresponds to the case $\varepsilon R_1 > 0$, while the minus sign corresponds to the case $\varepsilon R_1 < 0$. The expressions (34)–(35) provide some qualitative bifurcation results showing $|\varepsilon|$ versus R, which are presented in figure 4. We have assumed that initially $|\varepsilon|$ is sufficiently small. It should be noted that by the preferred convection pattern we mean the one that corresponds to the lowest value of R, which is often the case in the observation, and also agrees with the experimental expectation that the heat or solute transported by such a convection pattern, or equivalently the square of the convection amplitude ε^2, should increase with R. In fact, Iooss & Joseph (1980) have shown that those bifurcation branches for which the amplitude deceases with increasing R are probably not realizable. Hence, the results discussed in this paragraph may be useful to indicate the realization of a particular flow pattern if certain information about the values of R_1 and R_2 for such flow a pattern is available.

It is worth noting that in the case of non-zero R_1, which can correspond to the cases where convection is in the form of hexagons, both (34) and (35) for $|\varepsilon|$ can be applicable. For $R_1 = 0$, which can correspond to the cases of two-dimensional rolls, rectangles and square pattern convection, then the sign of R_2 determines whether the steady solution exists for values of R above or below R_0. For $R_1 = 0$ and supercritical convection, where $R > R_0$, the amplitude of convection increases with R and is largest, provided the value of R_2 is smallest among all the solutions to the nonlinear problem. For $R_1 = 0$ and subcritical convection, where $R < R_0$, the amplitude of convection decreases with increasing R and is largest, provided $|R_2|$ is smallest among all the solutions.

In the present problem, the coefficients R_1 and R_2 are due to the nonlinear convective terms in the temperature equation and the nonlinear interactions between the flow velocity and the non-uniform and nonlinear permeability associated with the perturbation to the basic-state liquid fraction.

It should also be noted that the variations of R_1 with respect to different parameters provide information about various destabilizing and stabilizing features for the

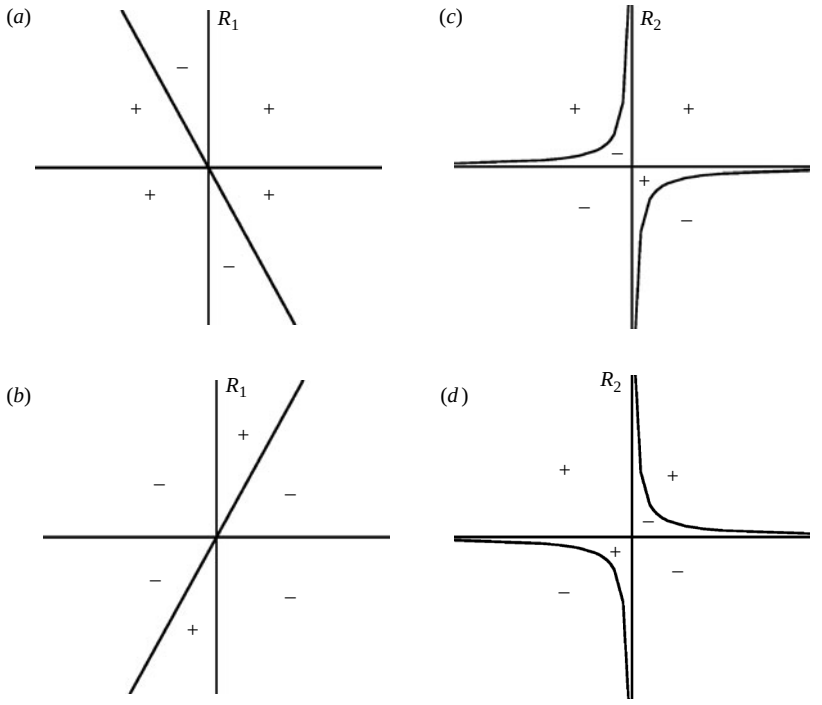

FIGURE 5. Bifurcation regions in the (ε, R_1)-plane for given $R_2 > 0$ (a) or $R_2 < 0$ (b) and in the (ε, R_2)-plane for given $R_1 > 0$ (c) or $R_1 < 0$ (d). Here the regions bounded by the solid lines and designated by a $+(-)$ indicate regions for supercritical (subcritical) bifurcation. For $R_1 = 0$, the supercritical (subcritical) region is the upper (lower) half-plane in the (ε, R_2)-plane.

hexagonal convection. However, the information about R_2 for the hexagons and non-hexagons is useful in the sense that since R_2 is the second-order coefficient in the expansion for R in powers of ε, R_2 plays useful roles in calculating the solute flux and the order of magnitude of ε in (34) and in the cases where R_1 is zero or becomes negligible.

To appreciate how R_1 and R_2 collectively lead to subcritical or supercritical bifurcations, figure 5 provides bifurcation regimes in the (ε, R_1)-space for given $R_2 > 0$ (figure 5*a*) or $R_2 < 0$ (figure 5*b*) and in the (ε, R_2)-space for given $R_1 > 0$ (figure 5*c*) or $R_1 < 0$ (figure 5*d*). In these figures, regions bounded by the solid lines and designated by a plus '+' sign indicate supercritical bifurcation regions, whereas those designated by a minus '—' sign indicate subcritical bifurcation regions. For $R_1 = 0$, the supercritical (subcritical) bifurcation region is the upper (lower) half-plane in the (ε, R_2)-space.

4.3. *Effect of the far-field temperature on the nonlinear system*

We now consider the cases of two- and three-dimensional convection near the onset of motion. In this paper, three types of non-hexagonal convection, where $R_1 = 0$, are considered in the form of two-dimensional rolls, three-dimensional rectangles with $\gamma = 45^\circ$ and squares, where the corresponding expressions for R_2 in the associated figures are designated by $R_2^{(r)}$, $R_2^{(ra)}$ and $R_2^{(s)}$, respectively. In figure 6, the results on the effect of θ_∞ on R_2 for rolls, rectangles and squares are shown. It can be seen that the variation in R_2 as θ_∞ is increased becomes more extreme in the case of squares, and subcritical rolls and rectangles exist over the whole range of the far-field temperature

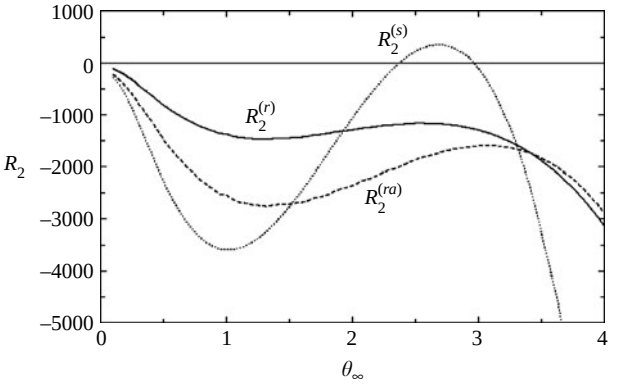

FIGURE 6. Variation of R_2 versus θ_∞ for non-hexagons with $S = 1$ and $C = 1$.

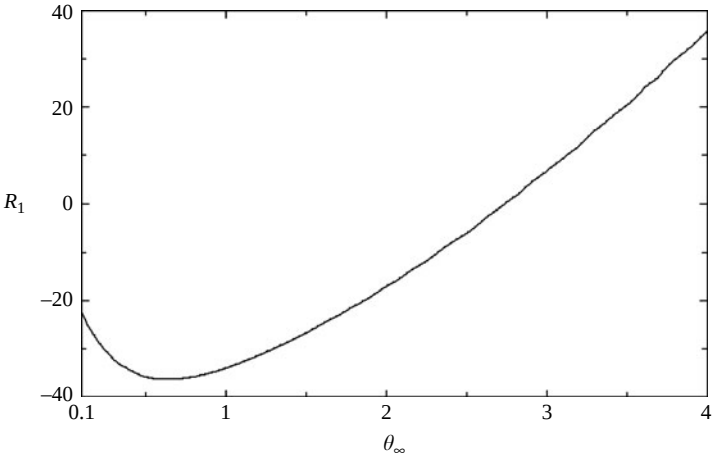

FIGURE 7. Variation of R_1 versus θ_∞ for hexagons with $C = 1$ and $S = 1$.

considered. However, in the case of squares, the results show that the flow can become supercritical for the values of θ_∞ between 2.370 and 2.962.

For the hexagonal solution, R_1 is plotted versus far-field temperature in figure 7. It is seen that R_1 changes sign as the far-field temperature is increased beyond some value. The results for the variation of R_2 versus far-field temperature are shown in figure 8. It is seen that $R_2 > 0$ for the values of θ_∞ between 1.795 and 3.275. Using the results shown in figures 4, 6 and 7, it can be concluded that realizable hexagons are possible for given values of the far-field temperature.

4.4. *Effect of the concentration ratio on the linear system*

We studied the effect of varying C by setting θ_∞ and S equal to one. Figure 9 presents variation of the mushy-layer depth with respect to C. Since the parameter C may be viewed as the non-dimensional parameter for the composition of the constituent dendrites formed during the solidification, increasing the composition of the constituent dendrites can increase the mushy-layer depth, as the results shown in this figure indicate. We also determined the results for the variations of R_0 and α versus C (figure 10). It can be seen from this figure that the flow is destabilized with increasing

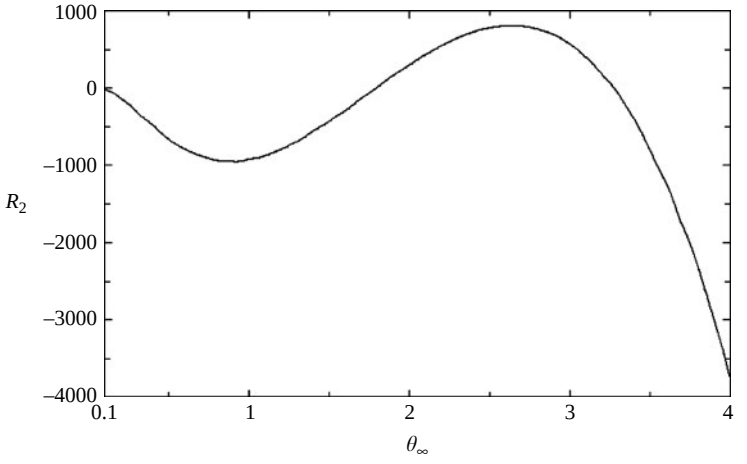

FIGURE 8. Variation of R_2 versus θ_∞ for hexagons with $C = 1$ and $S = 1$.

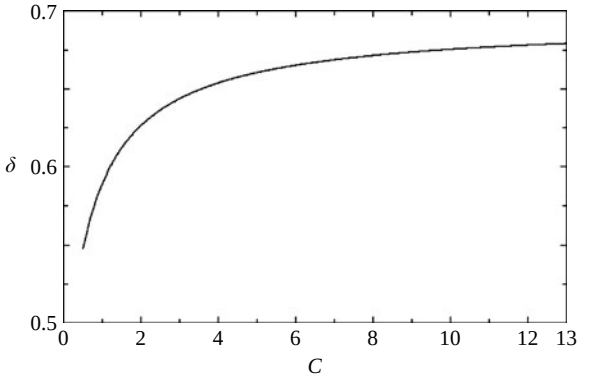

FIGURE 9. Variation of δ versus C for $S = 1$ and $\theta_\infty = 1$.

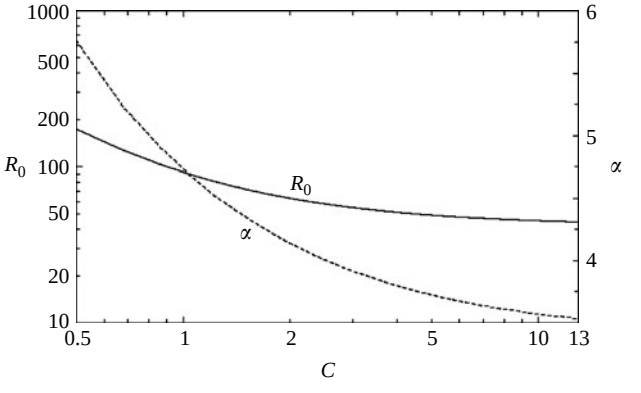

FIGURE 10. Variations of R_0 and α versus C for $S = 1$ and $\theta_\infty = 1$.

C, and the decrease in R_0 with increasing C agrees with the corresponding linear result reported in Worster (1992) for the two-layer system. The critical wavenumber also decreases with increasing C.

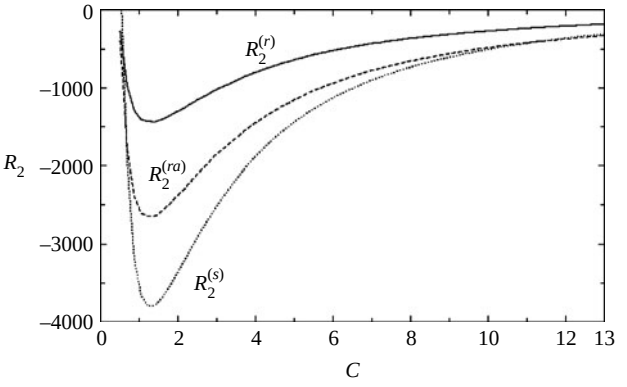

FIGURE 11. Variation of R_2 versus C for non-hexagons with $S=1$ and $\theta_\infty=1$.

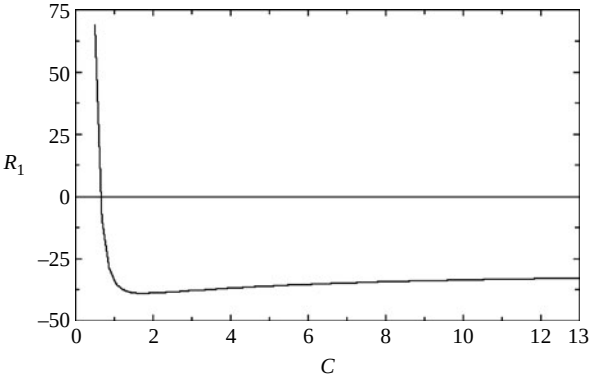

FIGURE 12. Variation of R_1 versus C for hexagons with $S=1$ and $\theta_\infty=1$.

4.5. *Effect of the concentration ratio on the nonlinear system*

For the non-hexagonal solutions ($R_1=0$), the results for the variation of R_2 versus C for $S=\theta_\infty=1$ are shown in figure 11. It can be seen that squares can be supercritical for $C\leqslant 0.5$, whereas the other two flow patterns are subcritical over the whole range of C considered. All three types of flow have a similar non-monotonic behaviour with respect to the variation with C.

For the hexagonal solutions, the results for the variation of R_1 versus C for $S=\theta_\infty=1$ are shown in figure 12. It can be seen that $R_1<0$ over most of the considered domain for C, but $R_1>0$ only for small values of C, which implies the possible existence of subcritical down-hexagons or supercritical up-hexagons in this range of values of C and for sufficiently small $|\varepsilon|$. The results for the variation of R_2 versus C for $S=\theta_\infty=1$ (figure 13) indicate that supercritical hexagons are not possible for $C>0.643$ and for $|\varepsilon|$ beyond some value. The coefficient R_2 decreases from $C=0.5$ to 1.587, but then tends to increase as concentration ratio is increased further.

4.6. *Effect of the Stefan number on the linear system*

We now hold both the far-field temperature and concentration ratio fixed equal to one and vary the Stefan number. Increasing S under these conditions decreases the

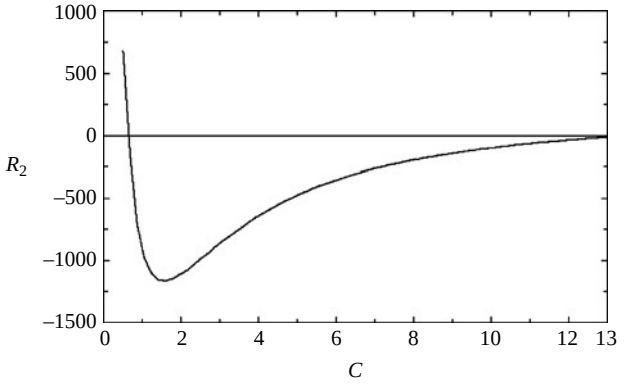

FIGURE 13. Variation of R_2 versus C for hexagons with $S = 1$ and $\theta_\infty = 1$.

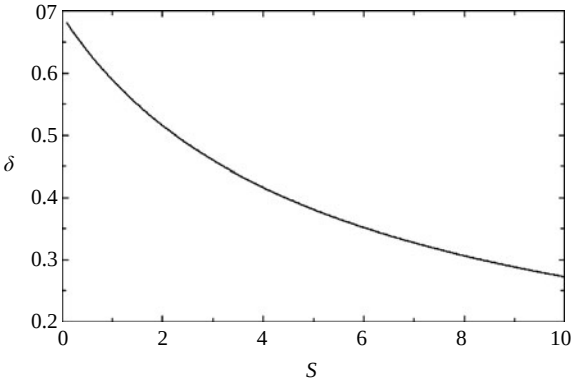

FIGURE 14. Variation of δ versus S for $C = 1$ and $\theta_\infty = 1$.

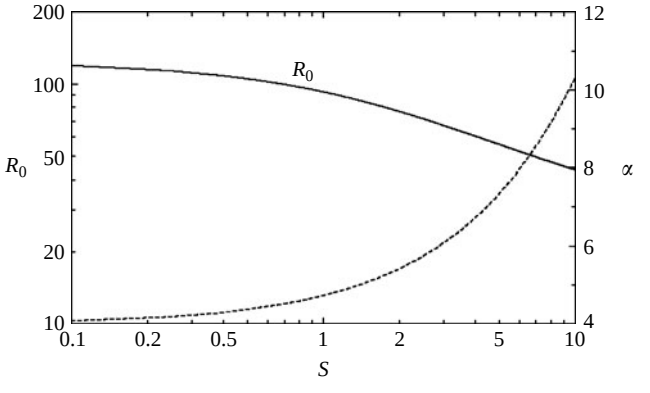

FIGURE 15. Variations of R_0 and α versus S for $C = 1$ and $\theta_\infty = 1$.

depth of the mushy layer (figure 14). Our results for the variation of the critical wavenumber and the Rayleigh number versus S (figure 15) indicate that α increases with S, while S has a destabilizing effect on the flow in the sense that R_0 decreases with increasing S.

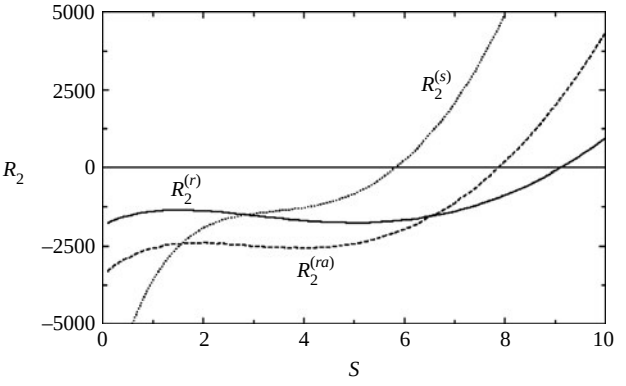

FIGURE 16. Variation of R_2 versus S for non-hexagons with $C = 1$ and $\theta_\infty = 1$.

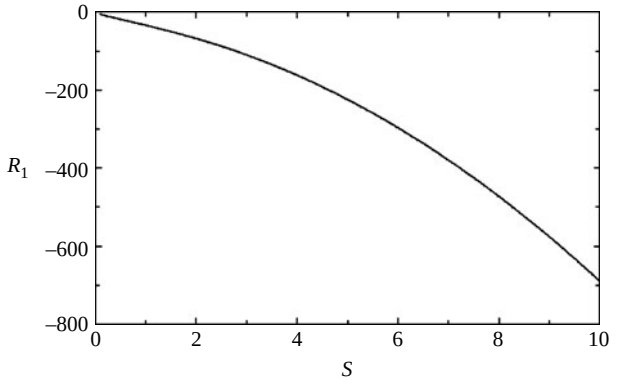

FIGURE 17. Variation of R_1 versus S for hexagons with $C = 1$ and $\theta_\infty = 1$.

4.7. *Effect of the Stefan number on the nonlinear system*

For the non-hexagonal solutions ($R_1 = 0$), the variation of R_2 versus S for $C = \theta_\infty = 1$ leads to the results (figure 16) that are briefly described as follows. Non-hexagonal flows may be subcritical or supercritical, depending on the value of S. Rolls can be subcritical when $S < 9.069$, rectangles when $S < 7.871$, and squares when $S < 5.817$. For large values of S, $R_2 > 0$, and the supercritical regime is enhanced for all these flow cases.

For the hexagonal convection, the variation of R_1 with respect to S for $C = \theta_\infty = 1$ (figure 17) indicates that R_1 is negative and monotonically decreases with increasing S. The variation of R_2 with respect to S for $C = \theta_\infty = 1$ is different (figure 18) in the sense that R_2 is positive for sufficiently large values of S and negative otherwise.

4.8. *Additional results of the present study*

In addition to the results presented and discussed in the previous subsections, which were the main outcome of the present study, we also determined some results about the values of the dependent variables as functions of the independent variables for different values of the parameters (Okhuysen 2005). The corresponding typical results are given here briefly as follows. The convective flow was found to exist at every horizontal level from top to bottom of the mushy layer. The results for the

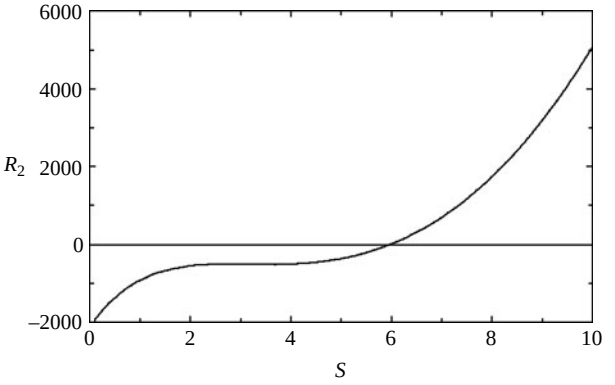

FIGURE 18. Variation of R_2 versus S for hexagons with $C = 1$ and $\theta_\infty = 1$.

liquid fraction indicated, in particular, relatively high values of liquid fraction in the neighbourhood of certain locations and extending from bottom to top of the mushy layer. Regions of high values of liquid fraction were surrounded by regions of relatively low liquid fraction. Such results indicate a tendency for chimney formation in the focused upflow regions, which reflect those determined for the chimneys by Chen & Chen (1991).

4.9. *Comparison with the previous weakly nonlinear studies*

Here, we first briefly describe the main features of the weakly nonlinear studies and the corresponding results due to Amberg & Homsy (1993), Anderson & Worster (1995) and Chung & Chen (2000), and then we compare the main features and the results of these to those of the present study.

The model treated in Amberg & Homsy (1993) assumes impermeable upper boundary, $\delta \ll 1$, $\theta_\infty \gg 1$, $C = O(1/\delta)$, $S = O(1)$, $\varepsilon = O(\delta)$ and a nearly constant case of the inverse of the permeability function in the form

$$\tilde{K} = 1 + K_1\phi + K_2\phi^2 + O(\phi^3), \quad \phi \equiv (1 - \chi) \leqslant O(\delta), \tag{36a, b}$$

where K_1 and K_2 are two constant parameters. Their linear problem yields the critical values for R_0 and α. For the nonlinear problem, only rolls up to $O(\varepsilon^2)$ ($R_1 = 0$, $R_2 \neq 0$) and hexagons up to order $\varepsilon(R_1 < 0)$ without any stability consideration were studied. They found that rolls were supercritical for sufficiently small values of K_1 and subcritical for K_1 beyond some value. Their hexagonal solution was found to be that of up-hexagons and bifurcated transcritically, which contradicts the experimental observations by Tait *et al.* (1992).

The model studied in Anderson & Worster (1995) assumes (36), impermeable upper boundary, $\delta \ll 1$, $\theta_\infty \gg 1$, $C = O(1/\delta)$, $S = O(1/\delta)$, $K_1 = O(\delta)$ and $\varepsilon \ll \delta \ll 1$. Their linear problem yields the critical values for R_0 and α. For the nonlinear problem, only rolls ($R_1 = 0$, $R_2 > 0$) and hexagons ($R_1 < 0$, $R_2 > 0$) up to order ε^2 were studied. The authors used their finite-amplitude solutions to derive an evolution equation, which was then used to investigate the stability of rolls and hexagons. They found that either up-hexagons or down-hexagons can be stable for sufficiently small $|\varepsilon|$, whereas rolls, which are supercritical, can become stable for larger $|\varepsilon|$. However, the parameter regime for the preference of down-hexagons was found to be significantly far from that observed experimentally (Tait *et al.* 1992).

The model treated in Chung & Chen (2000) assumes those of Anderson & Worster (1995), except that the permeable upper boundary is considered instead. Their linear problem yields the critical values for R_0 and α. For the nonlinear problem, they found similar results to those of Anderson & Worster (1995). However, even though the parameter regime for the preference of their detected down-hexagons was far from that observed experimentally, it was somewhat less far from the experimental value than that due to Anderson & Worster (1995). The main deficiencies of this model, as well as those earlier ones, have been the unrealistic features of small mushy-layer thickness, large far-field temperature and near-constant permeability. These unrealistic aspects of the model were partially recognized by Chung & Chen (2000) when they unsuccessfully attempted to add up terms in their series expansions in powers of δ in order to determine a more realistic result about the sense of the flow direction at the cell centres of the hexagons.

In the present study, we developed a realistic model by removing the assumptions posed in the previous models. Finite value for δ and arbitrary values for θ_∞, C and S are considered. The basic state and the linear problem yield δ, R_0, and α over a wide range of parameter values. Our linear results generally agree with those reported in the previous studies described above in the limits of small δ and large θ_∞. For the nonlinear problem, rolls ($R_1 = 0,\ R_2 \neq 0$), up-hexagons ($R_1 \neq 0,\ R_2 \neq 0$), down-hexagons ($R_1 \neq 0,\ R_2 \neq 0$), squares ($R_1 = 0,\ R_2 \neq 0$) and rectangles ($R_1 = 0,\ R_2 \neq 0$) up to $O(\varepsilon^2)$ were studied. We found that depending on the values of the parameters, supercritical or subcritical non-hexagons and hexagons are possible. Our nonlinear results in the parameter regime for small θ_∞, $C = S = 1$ and $\delta \sim 2$, which is close to the parameter regime of the experiments (Tait *et al.* 1992), indicate that the amplitude of any of the non-hexagonal solutions or up-hexagons decreases with increasing R, whereas the amplitude of the down-hexagons can increase with R. These results imply that any solution in the form of non-hexagons or up-hexagons is not preferred and is probably unstable, whereas the solution in the form of down-hexagons is the only detected solution, which is preferred and probably stable. These results of the present study are in agreement with a particular experimental observation due to Tait *et al.* (1992). For the case of small δ and large θ_∞, our nonlinear results agree with those of the previous weakly nonlinear studies in the case of hexagons since up-hexagons are preferred and down-hexagons are not preferred. Also, in this case, our result for rolls agrees with those of the previous weakly nonlinear studies since we found, in particular, a nonlinear solution in the form of subcritical rolls.

4.10. *Relation of present study to experiments*

In this paper, we were mainly concerned with a particular phenomenon that occurs when convection in the mushy layer does not become too vigorous. The convective flow that we investigated here is weak because our method of study is based on a weakly nonlinear theory. In addition, the analyses in the present study were for steady flow during steady-state solidification where the solidified material is pulled at a constant rate through a fixed temperature gradient. Consequently, we cannot expect to infer any results from the present study about the flow features in a mushy layer where chimneys are fully developed or transient conditions prevail. Thus, we are mostly interested in comparing the present results to those that can occur in experiments when convection in the mushy layer does not become too vigorous, although we are also interested in finding any possible relation between our present study and those of experiments, which were under transient or other conditions.

In the last several decades there have been a number of experimental studies of convection in mushy layers, notably those due to Copley *et al.* (1970), Chen & Chen (1991), Tait & Jaupart (1992), Chen (1995) and Aussillous *et al.* (2006), which were all performed under transient conditions, and the one due to Tait *et al.* (1992). Copley *et al.* (1970) were among the first to identify the primary instability of the fluid in the mushy layer, which is the one of interest here and investigated in the present paper.

Chen & Chen (1991) carried out experiments using 26 % ammonium chloride–water solutions. The convective flow was strong enough to lead to fully developed vertical chimneys within the mush, which were detected by using computer tomography. The authors found that chimneys extended all the way into the mushy layer, with little or no decrease in diameter. This result is in general agreement with the result of the present study about the existence of regions of high liquid fraction in the mushy layer.

Tait & Jaupart (1992) carried out solidification experiments using aqueous solutions of ammonium chloride with different viscosities, which allowed them to estimate a critical Rayleigh number R_m for some values of the far-field temperature and viscosities in the melt. Here R_m, which is related to R_0 by $R_m = \delta \Pi(\chi_m) R_0$, is defined based on the undisturbed depth of the mushy layer $\delta\kappa/V$ and the mean permeability of the layer $\Pi(\chi_m)\Pi(1)$, where χ_m is the mean porosity of the layer. Following Worster (1992), we used (7)–(8) and evaluated R_m for some values of the far-field temperature and found qualitative agreement with the corresponding experimental values obtained by Tait & Jaupart (1992). Explicitly, our quantitative comparison with the experimental values is briefly given as follows. Although figure 17 in Tait & Jaupart (1992) provides log-scale values of their porous medium Rayleigh number for different values of far-field temperature, we found it more convenient to make use of the experimental data points shown in figure 12 of Worster (1992) that were provided by Tait & Jaupart (1992). These experimental data points were collected for different viscosities of the melt used in the experiments. From these graphical points, we estimated value of R_m to be between 21 and 23 (viscosity: 5.0 mPa s) for $\theta_\infty = 0.1$, about 20 (viscosity: 16.0 mPa s) for $\theta_\infty = 0.13$, between 18 and 20 (viscosity: 9.0 mPa s) for $\theta_\infty = 0.6$ and between 16 and 18 (viscosity: 9.0 mPa s) for $\theta_\infty = 1.1$. The corresponding values for R_m in the present study are about 28.8, 27.0, 19.4 and 18.5, respectively. Our present result that mush thickness decreases with increasing far-field temperature is also in agreement with Tait & Jaupart's experimental result. These authors also observed that for melt at low viscosity, the chimneys penetrate all the way into the mushy layer and have a roughly constant diameter, whereas for melt at high viscosity the chimneys can broaden out into a 'root' structure. Our present result about regions of high liquid fraction is in agreement with their result for chimneys in the low-viscosity melt case, but not for the high-viscosity melt case. It should be noted that as Tait *et al.* (1992) suggested, in the experiments carried out by Tait & Jaupart (1992), the initial cooling of the base was not slow enough, so that the authors were not able to observe the initial stage of the flow pattern owing to the convection in the mushy layer.

The only experimental study that has been reported so far for weak convection in a mushy layer, which successfully detected the corresponding flow pattern, is that due to Tait *et al.* (1992). The experiments by these authors were designed with a much lower cooling rate than any other experiments, which probably gave instabilities more time to grow before the background temperature and the mush thickness had changed appreciably. These authors cooled and solidified a 28 % ammonium chloride–water

solution from below very slowly and carefully so that they were able to observe the onset of convection during the first stage of their experiments when the transient effects were negligible. They observed vertical, sheet-like upward flow forming along the sides of a roughly polygonal array. They carried out a statistical analysis of the number of nodes in the array and the lengths of sides of the polygons, and they found that among all possible plan forms, hexagons were closest to their results. The flow was found to be downward at the hexagonal cell centres and upward along the cell boundaries, where the crystals were dissolved to form chimneys. According to Tait *et al.* (1992), the flow pattern evolved with time as the mush thickened. Eventually, vertical chimneys formed at the nodes where the cell boundaries met, the branches disappeared and size of each cell increased notably. The formation of chimneys involved re-crystallization along the edges of the cells. The initial down-hexagonal planform that was observed in the first stage of their experiment, and was found to be a robust feature of the experiment, is in good agreement with our present results. We, in fact, found such a flow pattern to be the only realizable form of convection under similar conditions to those of Tait *et al.* It should be noted that in a down-hexagonal cell (Chandrasekhar 1961), downward motion occurs in a large central portion of the cell with maximum value of downward speed at the cell centre, whereas upward motion occurs close to the cell boundary with maximum value of upward speed at the vertices of the cell, which are the nodes where the cell boundaries meet. Tait *et al.* (1992) carefully took into account these standard properties of such hexagonal pattern (Busse 1978) and found that their observed flow pattern is closest to that for down-hexagons than to any other possible pattern.

Chen (1995) used a number of techniques to study experimentally the nature of convection in a mushy layer. Chen (1995) found that after chimneys were fully developed, downward convection toward the bottom took place followed by horizontal motion along the bottom toward the chimneys and then upward motion through chimneys. The results for the solid fraction indicated a significant decrease toward the bottom of the tank after chimneys were fully developed. However, the general characteristics of the solid fractions are comparable to those of the present study only in the region not too close to the lower boundary where the root system at the bottom of chimneys was found by Chen (1995). Although no quantitative or graphical results for the critical Rayleigh number were provided in Chen (1995), the author stated that his estimated value of the critical Rayleigh number was within a factor of 1.6 of the value found by Tait & Jaupart (1992), which is somewhat larger than that found in the present study.

Aussillous *et al.* (2006) carried out experiments using magnetic resonance imaging to study fully developed chimneys and convection in a mushy layer formed from an aqueous sucrose solution cooled from above. The viscosity of this aqueous solution increases strongly with the sucrose concentration and as temperature decreases. They found, in particular, that the chimneys do not span the full depth of the mushy layer, but they are visible only from 17 mm away from the cooling plate. If we interpret the chimneys as the regions of high porosity in our study, then the stated experimental result away from the cooling boundary is in general agreement with the present result. The convection in their experiment seems to be limited only to the lower section of the mushy layer, while convective flow in the mushy layer of the present study has no such limitation. These partial differences are expected to be due the fact that the fluid in these experiments has strong temperature and concentration-dependent viscosity and these experiments are for the transient flow regime where chimneys are fully

developed, while the present study is for constant-viscosity fluid and for weak steady convection, where no chimney is fully developed.

5. Conclusion and remarks

We investigated the problem of weakly nonlinear buoyant convection in mushy layers during alloy solidification for a permeable mush–liquid interface. We developed a new model for the problem, which is more realistic than those developed in the past and is relevant for mushy layers with finite thickness and for arbitrary values of the parameters, such as far-field temperature, concentration ratio and Stefan number. We analysed the effects of several parameters on two- and three-dimensional steady convection cases. Using both analytical and numerical methods, we determined the steady solutions of the weakly nonlinear problem in different ranges of the values of the parameters. We found that depending on the range of values of the parameters, bifurcation to hexagon or non-hexagon pattern convection can be either supercritical or subcritical. Among all the solutions detected, there are those whose amplitudes increase with R, which we label as realizable solutions, and those whose amplitudes decrease with increasing R, which are probably unstable and, thus, not physically realizable.

The most important result of the present study was the prediction of realizable convection with down-hexagonal pattern, which was observed by Tait *et al.* (1992), and our prediction of such a flow pattern was under particular conditions and range of the values of the parameters that cover those of the same experiment by Tait *et al.* (1992). Over the same particular conditions and range of parameter values, we found that all the other predicted solutions in the form of rolls, squares, rectangles or up-hexagons are not realizable and probably unstable since their amplitudes decrease with increasing R.

The present results are based on our newly developed model, which is applicable to mushy layers with finite thickness δ and for arbitrary values of the parameters, such as the far-field temperature θ_∞, the concentration ratio C and the Stefan number S. The previous analytical studies (Amberg & Homsy 1993; Anderson & Worster 1995; Chung & Chen 2000) were all based on the limit of large far-field temperature ($\theta_\infty \gg 1$) and small mushy-layer thickness ($\delta \ll 1$). The authors of these previous studies attempted to compare their results with those of the experiment by Tait *et al.* (1992), but mostly no significant agreement was found because the experimental observations were for $\delta = O(1)$ and $\theta_\infty \ll 1$, which were sharply different from those assumed in the previous analytical studies. For example, Chung & Chen (2000) concluded preference of up-hexagons in the parameter regime where Tait *et al.* (1992) observed down-hexagons. Chung & Chen (2000) recognized that a future improvement of their model could be to lift the condition of small $\delta(\delta \ll 1)$. However, we detected that in addition to finite-δ values, which has been important for the present model, the small value of θ_∞ has been significant too for the prediction of the experimental results since we found that the results for $\theta_\infty \gg 1$ can be quite different from those for $\theta_\infty \ll 1$.

As discussed in the previous section, the convection in the mushy layer that was observed by Tait *et al.* (1992), was initially in the form of down-hexagons, where transient effects were negligible, but later as the thickness of the mushy layer thickened sufficiently, the pattern changed into a new structure where in each hexagonal cell, upward motion occurred along six chimneys at the cell's six nodes and downward motion remained similar to that for a down-hexagonal cell. Our present

theory predicted only the initial flow pattern observed by Tait *et al.* (1992), which existed for limited values of the mush thickness when the transient effects did not become significant. This restriction for the theoretical prediction may well be related to an important difference between the typical experiments and weakly nonlinear theories. The typical experiments examine time-dependent solidification with a fixed cooled base and time-dependent mushy layer thickness, and time-dependent effects can become significant when the value of mush thickness increases sufficiently, raising the value of the effective Rayleigh number beyond some value. However, the theories have been for steady solidification at constant speed of a mushy layer with constant thickness and sufficiently low values of the Rayleigh number. It is hoped that in future, new types of nonlinear theories can be developed that can deal with time-dependent solidification problems such as the one explained here, which could lead to more predictions of the experimental results.

Finally, in regard to the stability of the finite-amplitude flow solutions predicted in the present study, it should be noted that the present perturbation approach is generally incapable of carrying out a standard stability analysis (Busse 1967) because the asymmetries in the present problem, which cause non-zero values for R_1, are, in general, not small. A stability investigation, which requires extensive work and remains a topic for future study, will require full numerical computation of both finite-amplitude solutions and their stability analysis without using the perturbation approach.

Appendix

The expressions for the 3×3 matrix operators $\boldsymbol{L}$ and $\boldsymbol{L}'$ and the vector operator $\boldsymbol{N}$ are

$$\boldsymbol{L} = (row_1, row_2, row_3)^T, \tag{A 1a}$$

where row_i $(i = 1, 2, 3)$ is the ith row of the matrix $\boldsymbol{L}$ and given by

$$\begin{aligned} row_1 &\equiv \{(\partial/\partial t - \partial/\partial z - \nabla^2), [S(\partial/\partial t - \partial/\partial z)], [-(\mathrm{d}\theta_b/\mathrm{d}z)\Delta_2]\}, \\ row_2 &\equiv \{[\chi_b(\partial/\partial t - \partial/\partial z) - \mathrm{d}\chi_b/\mathrm{d}z], [(\theta_b - C)(\partial/\partial t - \partial/\partial z) - \mathrm{d}\theta_b/\mathrm{d}z], [-(\mathrm{d}\theta_b/\mathrm{d}z)\Delta_2]\}, \\ row_3 &\equiv \{ - RK_b^{-1}\Delta_2, 0, [(\nabla^2 + K_b^{-1}\mathrm{d}K_b/\mathrm{d}z\partial/\partial z)\Delta_2]\}, \end{aligned} \tag{A 1b–d}$$

and

$$\boldsymbol{L}' = (row_1', row_2', row_3')^T, \tag{A 2a}$$

where $row_i'(i = 1, 2, 3)$ is the ith row of the matrix $\boldsymbol{L}'$ and given by

$$row_1' \equiv 0, row_2' \equiv 0, row_3' \equiv (K_b^{-1}\Delta_2, 0, 0), \tag{A 2b–d}$$

and

$$\begin{aligned} \boldsymbol{N}(\boldsymbol{q}, \boldsymbol{q}) = -\{&[(\Omega P)\cdot\nabla\theta], [(\Omega P)\cdot\nabla\theta + \chi(\partial/\partial t - \partial/\partial z)\theta \\ &+ \theta(\partial/\partial t - \partial/\partial z)\chi], K_b^{-1}[(\partial/\partial z)(\nabla K\cdot\Omega P) + \nabla^2(K\Delta_2 P)]\}^T. \end{aligned} \tag{A 3}$$

The expression of the 3×3 matrix differential operator $\boldsymbol{L}^{(a)}$ is

$$\boldsymbol{L}^{(a)} = [row_1^{(a)}, row_2^{(a)}, row_3^{(a)}]^T, \tag{A 4a}$$

where $row_i^{(a)}$ is the ith row of the matrix $\boldsymbol{L}^{(a)}$ and given by

$$\begin{aligned} row_1^{(a)} &\equiv [(\mathrm{D}^2 - \mathrm{D} - \tilde{\alpha}^2), -\chi_b\mathrm{D}, -\tilde{R}_0K_b^{-1}], \quad row_2^{(a)} \equiv [SD, (\theta_b - C)D, 0], \\ row_3^{(a)} &\equiv \{-\mathrm{d}\theta_b/\mathrm{d}z, -\mathrm{d}\theta_b/\mathrm{d}z, [\mathrm{D}^2 - K_b^{-1}\mathrm{d}K_b/\mathrm{d}z\mathrm{D} - K_b^{-2}(\mathrm{d}^2K_b/\mathrm{d}z^2K_b \\ &\quad - \mathrm{d}K_b/\mathrm{d}z\mathrm{d}K_b/\mathrm{d}z + \tilde{\alpha}^2)]\}, \end{aligned} \tag{A 4b}$$

and the boundary conditions $\boldsymbol{B}^{(a)}$ mean

$$\tilde{\theta}_0^{(a)} = \tilde{P}_0^{(a)} = \tilde{\chi}_0^{(a)} = 0 \text{ at } z = 0, \quad \tilde{\theta}_0^{(a)} = \left(D - \mathrm{d}K_b/\mathrm{d}z K_b^{-1}\right)\tilde{P}_0^{(a)} = 0 \text{ at } z = \delta. \quad (\mathrm{A}\,4c, d)$$

REFERENCES

Amberg, G. & Homsy, G. M. 1993 Nonlinear analysis of buoyant convection in binary solidification with application to channel formation. *J. Fluid Mech.* **252**, 79–98.

Anderson, D. M. & Worster, M. G. 1995 Weakly nonlinear analysis of convection in mushy layers during the solidification of binary alloys. *J. Fluid Mech.* **302**, 307–331.

Ascher, U. M., Mattheij, R. M. & Russell, R. D. 1995 *Numerical Solution of Boundary Value Problems for Ordinary Differential Equations*, 2nd edn. SIAM, Philadelphia.

Aussillous, P., Sederman, A. J., Gladen, L. F., Huppert, H. E. & Worster, M. G. 2006 Magnetic resonance imaging of structure and convection in solidifying mushy layers. *J. Fluid Mech.* **552**, 99–125.

Busse, F. H. 1967 The stability of finite-amplitude convection and its relation to an extremum principal. *J. Fluid Mech.* **30**, 625–649.

Busse, F. H. 1978 Nonlinear properties of thermal convection. *Rep. Prog. Phys.* **41**, 1929–1967.

Chandrasekhar, S. 1961 *Hydrodynamic and Hydromagnetic Stability*. Clarendon.

Chen, F. 1995 Experimental study of convection in a mushy layer during directional solidification. *J. Fluid Mech.* **293**, 81–98.

Chen, F. & Chen, C. F. 1991 Experimental study of directional solidification of aqueous ammonium chloride solution. *J. Fluid Mech.* **227**, 567–586.

Chen, F., Lu, J. W. & Yang, T. L. 1994 Convective instability in ammonium chloride solution directionally solidified from below. *J. Fluid Mech.* **276**, 163–187.

Chung, C. & Chen, F. 2000 Onset of plume convection in mushy layers. *J. Fluid Mech.* **408**, 53–82.

Copley, S. M., Giamei, A. F., Johnson, S. M. & Hornbecker, M. F. 1970 The origin of freckles in unidirectionally solidified casting. *Metall. Trans.* **1**, 2193–2204.

Emms, P. & Fowler, A. 1994 Compositional convection in the solidification of binary alloys. *J. Fluid Mech.* **262**, 111–139.

Fowler, A. C. 1985 The formation of freckles in binary alloys. *IMA J. Appl. Maths* **35**, 159–174.

Hills, R., Loper, D. & Roberts, P. 1983 A thermodynamically consistent model of a mushy zone. *Q. J. Mech. Appl. Maths.* **36**, 505–539.

Iooss, G & Joseph, D. D. 1980 *Elementary Stability and Bifurcation Theory*. Springer.

Joseph, D. D. 1976 *Stability of Fluid Motions*. Springer.

Keller, H. B. 1976 *Numerical Solution of Two Point Boundary Value Problems*. SIAM, Philadelphia.

Lage, J. 1998 The fundamental theory of flow through permeable media from Darcy to turbulence. In *Transport Phenomena in Porous Media* (ed. D. Ingham & I. Pop), pp. 1–30. Pergamon.

Okhuysen, B. S. 2005 Analytical and computational studies of convection in solidifying binary media. PhD thesis, Department of Theoretical and Applied Mechanics, University of Illinois at Urbana-Champaign, USA.

Tait, S. & Jaupart, C. 1992 Compositional convection in a reactive crystalline mush and melt differentiation. *J. Geophys. Res.* **97**, 6735–6756.

Tait, S., Jahrling, K. & Jaupart, C. 1992 The planform of compositional convection and chimney formation in a mushy layer. *Nature* **359**, 406–408.

Worster, M. G. 1991 Natural convection in a mushy layer. *J. Fluid Mech.* **224**, 335–359.

Worster, M. G. 1992 Instabilities of the liquid and mushy regions during solidification of alloys. *J. Fluid Mech.* **237**, 649–669.